Highly reflective Bragg gratings in slightly etched step-index polymer optical fiber

Xuehao Hu,[1] Chi-Fung Jeff Pun,[2] Hwa-Yaw Tam,[2] Patrice Mégret,[1] and Christophe Caucheteur[1,*]

[1]*Electromagnetism and Telecommunication Department, Université de Mons, 31 Boulevard Dolez, Mons, 7000, Belgium*

[2]*Department of Electrical Engineering, The Hong Kong Polytechnic University, Hong Kong, China*

[*]*christophe.caucheteur@umons.ac.be*

Abstract: During the past few years, a strong progress has been made in the photo-writing of fiber Bragg gratings (FBGs) in polymer optical fibers (POFs), animated by the constant wish to enhance the grating reflectivity and improve the sensing performances. In this paper, we report the photo-inscription of highly reflective gratings in step-index POFs, obtained thanks to a slight etching of the cladding. We demonstrate that a cladding diameter decrease of ~12% is an ideal trade-off to produce highly reflective gratings with enhanced axial strain sensitivity, while keeping almost intact their mechanical resistance. For this, we make use of Trans-4-stilbenemethanol-doped photosensitive step-index poly(methyl methacrylate) (PMMA) POFs. FBGs are inscribed at ~1550 nm by the scanning phase mask technique in POFs of different external diameters. Reflectivity reaching 97% is achieved for 6 mm long FBGs, compared to 25% for non-etched POFs. We also report that a cladding decrease enhances the FBG axial tension while keeping unchanged temperature and surrounding refractive index sensitivities. Finally and for the first time, a measurement is conducted in transmission with polarized light, showing that a photo-induced birefringence of 7×10^{-6} is generated (one order of magnitude higher than the intrinsic fiber birefringence), which is similar to the one generated in silica fiber using ultra-violet laser.

OCIS codes: (060.2370) Fiber optics sensors; (060.3735) Fiber Bragg gratings.

References and links

1. Z. Xiong, G. D. Peng, B. Wu, and P. L. Chu, "Highly tunable Bragg gratings in single-mode polymer optical fibers," IEEE Photon. Technol. Lett. **11**(3), 352–354 (1999).
2. A. Stefani, M. Stecher, G. E. Town, and O. Bang, "Direct writing of fiber Bragg grating in microstructured polymer optical fiber," IEEE Photon. Technol. Lett. **24**(13), 1148–1150 (2012).
3. D. J. Webb, K. Kalli, K. Carroll, C. Zhang, M. Komodromos, A. Argyros, M. Large, G. Emiliyanov, O. Bang, and E. Kjaer, "Recent developments of Bragg gratings in PMMA and TOPAS polymer optical fibers," Proc. SPIE **6830**, 683002 (2008).
4. G. Statkiewicz-Barabach, K. Tarnowski, D. Kowal, P. Mergo, and W. Urbanczyk, "Fabrication of multiple Bragg gratings in microstructured polymer fibers using a phase mask with several diffraction orders," Opt. Express **21**(7), 8521–8534 (2013).
5. H. Dobb, D. J. Webb, K. Kalli, A. Argyros, M. C. J. Large, and M. A. van Eijkelenborg, "Continuous wave ultraviolet light-induced fiber Bragg gratings in few- and single-mode microstructured polymer optical fibers," Opt. Lett. **30**(24), 3296–3298 (2005).
6. X. Chen, C. Zhang, D. J. Webb, G. D. Peng, and K. Kalli, "Bragg grating in a polymer optical fibre for strain, bend and temperature sensing," Meas. Sci. Technol. **21**(9), 094005 (2010).
7. C. A. F. Marques, L. B. Bilro, N. J. Alberto, D. J. Webb, and R. N. Nogueira, "Inscription of narrow bandwidth Bragg gratings in polymer optical fibers," J. Opt. **15**(7), 075404 (2013).
8. W. Yuan, A. Stefani, and O. Bang, "Tunable polymer fiber Bragg grating (FBG) inscription: fabrication of dual-FBG temperature compensated polymer optical fiber strain sensors," IEEE Photon. Technol. Lett. **24**(5), 401–403 (2012).

#210487 - $15.00 USD Received 21 Apr 2014; revised 9 Jul 2014; accepted 13 Jul 2014; published 25 Jul 2014

9. K. E. Carroll, C. Zhang, D. J. Webb, K. Kalli, A. Argyros, and M. C. J. Large, "Thermal response of Bragg gratings in PMMA microstructured optical fibers," Opt. Express **15**(14), 8844–8850 (2007).
10. H. Y. Liu, G. D. Peng, and P. L. Chu, "Thermal tuning of polymer optical fiber Bragg gratings," IEEE Photon. Technol. Lett. **13**(8), 824–826 (2001).
11. W. Yuan, A. Stefani, M. Bache, T. Jacobsen, B. Rose, N. Herholdt-Rasmussen, F. K. Nielsen, S. Andresen, O. B. Sørensen, K. S. Hansen, and O. Bang, "Improved thermal and strain performance of annealed polymer optical fiber Bragg gratings," Opt. Commun. **284**(1), 176–182 (2011).
12. Z. F. Zhang, C. Zhang, X. M. Tao, G. F. Wang, and G. D. Peng, "Inscription of polymer optical fiber Bragg grating at 962 nm and its potential in strain sensing," IEEE Photon. Technol. Lett. **22**(21), 1562–1564 (2010).
13. X. Hu, D. Kinet, K. Chah, P. Mégret, and C. Caucheteur, "Bragg gratings inscription at 1550 nm in photosensitive step-index polymer optical fiber," Proc. SPIE **8794**, 87942Q (2013).
14. A. Stefani, S. Andresen, W. Yuan, N. Herholdt-Rasmussen, and O. Bang, "High sensitivity polymer optical fiber-Bragg-grating-based accelerometer," IEEE Photon. Technol. Lett. **24**(9), 763–765 (2012).
15. W. Yuan, L. Khan, D. J. Webb, K. Kalli, H. K. Rasmussen, A. Stefani, and O. Bang, "Humidity insensitive TOPAS polymer fiber Bragg grating sensor," Opt. Express **19**(20), 19731–19739 (2011).
16. C. Markos, A. Stefani, K. Nielsen, H. K. Rasmussen, W. Yuan, and O. Bang, "High-T_g TOPAS microstructured polymer optical fiber for fiber Bragg grating strain sensing at 110 degrees," Opt. Express **21**(4), 4758–4765 (2013).
17. I. P. Johnson, W. Yuan, A. Stefani, K. Nielsen, H. Rasmussen, L. Khan, D. J. Webb, K. Kalli, and O. Bang, "Optical fibre Bragg grating recorded in TOPAS cyclic olefin copolymer," IEEE Electron. Lett. **47**(4), 271–272 (2011).
18. Z. F. Zhang and X. M. Tao, "Synergetic effects of humidity and temperature on PMMA based fiber Bragg gratings," J. Lightwave Technol. **30**(6), 841–845 (2012).
19. W. Zhang, D. Webb, and G. Peng, "Polymer optical fiber Bragg grating acting as an intrinsic biochemical concentration sensor," Opt. Lett. **37**(8), 1370–1372 (2012).
20. C. Zhang, X. Chen, D. J. Webb, and G. D. Peng, "Water detection in jet fuel using a polymer optical fibre Bragg grating," Proc. SPIE **7503**, 750380 (2009).
21. G. Rajan, M. Y. M. Noor, N. H. Lovell, E. Ambikaizrajah, G. Farrell, and G. D. Peng, "Polymer micro-fiber Bragg grating," Opt. Lett. **38**(17), 3359–3362 (2013).
22. G. Rajan, Y. M. Noor, B. Liu, E. Ambikairaja, D. J. Webb, and G. D. Peng, "A fast response intrinsic humidity sensor based on an etchedsinglemode polymer fiber Bragg grating," Sens. Actuators A Phys. **203**, 107–111 (2013).
23. G. Rajan, B. Liu, Y. Luo, E. Ambikairajah, and G. D. Peng, "High sensitivity force and pressure measurements using etched singlemode polymer fiber Bragg gratings," IEEE Sens. J. **13**(5), 1794–1800 (2013).
24. D. Sáez-Rodríguez, K. Nielsen, H. K. Rasmussen, O. Bang, and D. J. Webb, "Highly photosensitive polymethyl methacrylate microstructured polymer optical fiber with doped core," Opt. Lett. **38**(19), 3769–3772 (2013).
25. H. Y. Liu, H. B. Liu, G. D. Peng, and P. L. Chu, "Observation of type I and type II gratings behavior in polymer optical fiber," Opt. Commun. **220**(4), 337–343 (2003).
26. H. B. Liu, H. Y. Liu, G. D. Peng, and P. L. Chu, "Novel growth behaviors of fiber Bragg gratings in polymer optical fiber under UV irradiation with low power," IEEE Photon. Technol. Lett. **16**(1), 159–161 (2004).
27. F. Lhommé, C. Caucheteur, K. Chah, M. Blondel, and P. Mégret, "Synthesis of fiber Bragg grating parameters from experimental reflectivity: a simplex approach and its application to the determination of temperature-dependent properties," Appl. Opt. **44**(4), 493–497 (2005).
28. A. Stefani, W. Yuan, C. Markos, and O. Bang, "Narrow bandwidth 850-nm fiber Bragg gratings in few-mode polymer optical fibers," IEEE Photon. Technol. Lett. **23**(10), 660–662 (2011).
29. C. Caucheteur, S. Bette, R. Garcia-Olcina, M. Wuilpart, S. Sales, J. Capmany, and P. Mégret, "Transverse strain measurements using the birefringence effect in fiber Bragg gratings," IEEE Photon. Technol. Lett. **19**(13), 966–968 (2007).
30. C. Caucheteur, S. Bette, R. Garcia-Olcina, M. Wuilpart, S. Sales, J. Capmany, and P. Mégret, "Influence of the grating parameters on the polarization properties of fiber Bragg gratings," J. Lightwave Technol. **27**(8), 1000–1010 (2009).

1. Introduction

Fiber Bragg gratings (FBGs) were first fabricated in polymer optical fibers (POFs) in 1999 [1]. Since then, through the use of different fiber types and inscription processes, a strong progress has been realized towards the realization of high quality gratings. Polymer optical FBGs have been photo-inscribed point-by-point (fourth order gratings) [2] and with the phase mask technique, either under static exposition [3–5] or laser beam scanning along the phase mask [6,7]. FBGs inscribed in POFs present several attractive features for sensing purposes. Compared to their counterparts produced in silica fibers, they are more sensitive to temperature, strain and acceleration, because of the larger thermo-optic coefficient and smaller Young's modulus of polymer materials [8–14]. Although different polymer materials

#210487 - $15.00 USD Received 21 Apr 2014; revised 9 Jul 2014; accepted 13 Jul 2014; published 25 Jul 2014

can be used to manufacture POFs [15–17], the most often encountered one is poly(methyl methacrylate) (PMMA). Unlike silica, PMMA demonstrates absorption of moisture up to 2 w.t. %, so that PMMA FBGs can be used as humidity sensors [18], biochemical concentration sensors [19] or water detection sensors [20].

The etching technique for PMMA POFs has been recently developed by Peng's group. POFs were strongly etched and then tapered to reduce the diameter from 253 μm to 16 μm (up to more than 90% of the initial value), which decreases the inscription time with static laser beam because of more effective power absorption in the core of the fiber. At the same time the reflectivity decreases by 90% because of the etching and tapering process [21]. It was then demonstrated that gratings produced in etched POFs present enhanced humidity and tension sensitivities compared to pristine fibers [22,23]. However, the remaining diameter is so thin that such etched POFs are not convenient to handle and are very fragile. In this work, we demonstrate that slightly etched POF to a diameter decrease of 12% constitutes an ideal compromise to produce strongly reflective gratings (> 95%) with enhanced axial tension sensitivity while keeping almost unchanged the initial mechanical resilience.

The fibers used in this work were manufactured at the *Hong Kong Polytechnic University*. They are characterized by a core diameter of 8.2 μm and a cladding diameter of ~150 μm. The cladding is in pure PMMA while the core is composed of PMMA doped with Diphenyl sulfide (5% mole) and Trans-4-stilbenemethanol (1% w.t.). Highly-reflective uniform FBGs were photo-inscribed in a POF using a Helium-Cadmium laser emitting at 325 nm with the scanning phase mask technique [24–26]. During the inscription process, we have monitored the evolution of FBGs amplitude reflected spectra, allowing us to evaluate the dynamics of bandwidth modification and central wavelength shift. Then, FBGs inscribed in POFs of different diameters were subjected to temperature changes in the range [20-50 °C], axial strain changes in the range [0-0.06 N] and surrounding refractive index changes in the range [1.33-1.37]. These characterizations confirm that a cladding decrease enhances the axial strain sensitivity, while maintaining the temperature and surrounding refractive index change sensitivities. In our work, the splicing between POF and silica fibers was optimized through the use of acrylic sealant in addition to the UV-curing adhesive. This allows us to obtain a waterproof connection with an enhanced strength. Finally, measurements with polarized light have been conducted in transmission on a uniform FBG characterized by a 16 dB rejection band. The polarization dependent loss (PDL) spectrum depicts a maximum at 1.7 dB, allowing to estimate that the photo-induced birefringence resulting from the side inscription process is 7×10^{-6}, which is one order of magnitude higher than the intrinsic fiber birefringence. This value was computed thanks to a numerical fit of the experimental data using an in-house developed inverse scattering program based on the Nelder-Mead simplex algorithm, as reported in [27].

In the remaining of the paper, we first detail all the processes to handle POFs for FBGs writing, comprising the etching process, the splicing method and the photo-writing technique. We then focus on experimental evolutions recorded during the writing process and in response to different external solicitations.

2. Experiments

2.1 Etching process of POFs

POFs were etched by immersion in a mixture of acetone and methanol (ratio 2:1). A calibration process revealed that the etching rate is equal to 3.44 μm/minute. Figure 1(a) shows the evolution of POF diameter when being etched. The diameter was evaluated from pictures taken by a microscope Nikon 100s. Figure 1(b) shows optical microscope pictures of the POF after 5 minutes and 30 minutes of the etching process. The corresponding remaining diameters are 133 μm and 49 μm, respectively. More importantly, the cylindrical shape of the fiber is maintained, whatever the diameter values.

#210487 - $15.00 USD Received 21 Apr 2014; revised 9 Jul 2014; accepted 13 Jul 2014; published 25 Jul 2014

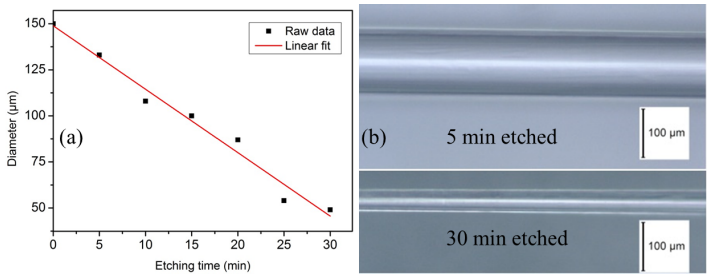

Fig. 1. Evolution of the cladding diameter during the etching process (a) and microscope pictures at two times during the etching process (b).

2.2 Photo-inscription process of the FBGs

The laser used in this work is a He-Cd laser (Kimmon IK5751I-G) with an output power of 30 mW at 325 nm. The output beam width of the laser is 1.2 mm. Figure 2(a) depicts the experimental set-up.

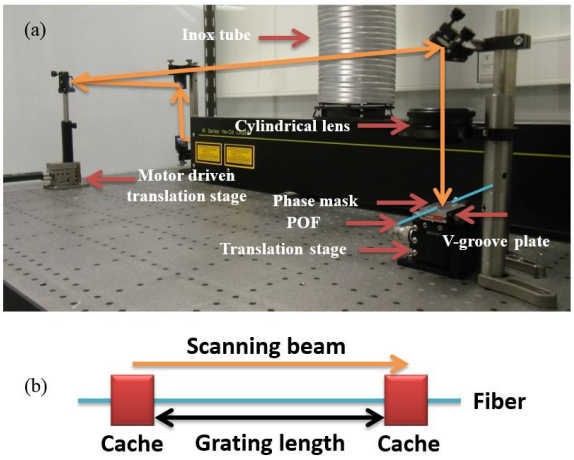

Fig. 2. Experimental set-up for FBG photo-inscription in POFs (a) and sketch of the scanning laser beam technique along the fiber axis (b).

The inox tube positioned above the laser allows evacuating the air turbulences caused by the cooling system, avoiding them to perturb the photo-writing process. The UV beam emitted by the laser was reflected by four mirrors (even number of reflections to preserve the output state of polarization) towards the POF, which was hold in a V-groove plate. A uniform phase mask (Coherent) with a period of 1044 nm was placed above the fiber as closely as possible. A cylindrical lens with 10 cm focal length was used in front of the phase mask to focus the UV beam on the fiber core. The movement of the third mirror was controlled by a motor-driven translation stage, which was used to scan the laser along the fiber over a maximum length of 20 mm. To ensure a uniform refractive index modulation profile, a cache whose aperture is equal to the desired grating length was placed above the fiber and the laser beam scan was started and stopped over the cache, as illustrated in Fig. 2(b). Amplitude reflected spectrum measurements were obtained with an FBG interrogator (FS2200SA from FiberSensing), which presents a wavelength resolution of 1 pm and a scanning rate of 1 Hz.

2.3 Splicing of the POF sections with silica fibers

The loss of this step-index POF is quite high. With the cut-back technique, it has been measured equal to ~3 dB/cm at 1550nm [28]. So in our experiments, only a few centimeters

#210487 - $15.00 USD Received 21 Apr 2014; revised 9 Jul 2014; accepted 13 Jul 2014; published 25 Jul 2014

of POFs were used. For quality evaluation during the inscription process, POF sections were connected to standard silica single-mode optical fiber pigtails with index matching gel. Then, to carry out experiments after the inscription process, POF sections containing FBGs were UV-glued (Norland 78) to two 8° angled silica fiber pigtails on both sides of POF. The index matching UV-glue used between fibers could avoid Fabry–Perot cavity effects and the angled silica fiber could reduce the Fresnel reflections generated in the interface between silica fiber and UV-glue because of large refractive index difference between cured UV-glue (refractive index 1.48) and silica fiber. Figure 3(a) displays a picture of the splice obtained in these conditions.

As provided by the manufacturer, the tensile strength of the UV-glue is 649 psi after curing. Because the splice is the weakest part in polymer optical FBG applications, we have further optimized the strength of the splicing part, similar to [14]. For this, acrylic sealant was dip-coated on the UV-glue splice, as shown in Fig. 3(b), which made the splice waterproof and much more resistant (although the exact tensile strength has not been computed).

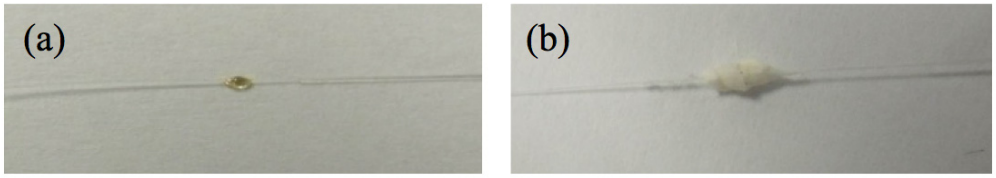

Fig. 3. UV cured splice without acrylic sealant coating (a) and UV cured splice with acrylic sealant coating (b) between POF and angled silica fiber.

3. Experimental results

3.1 Dynamic recording of the reflected spectra during the inscription process

Figure 4 depicts the kinetic growth of a non-etched FBG manufactured by the scanning phase mask technique. The scanning velocity was chosen equal to 3 µm/s, yielding a 6 mm long grating after 40 minutes of writing according to the laser beam width and the use of a cache at both sides of the grating region, as depicted in Fig. 2(b). At the end of the writing process, the maximum amplitude of the reflection band is > 20 dB above the mean noise level. During the growth, the full width at half maximum (FWHM) decreases from 810 pm down to 130 pm, due to the increase of the FBG physical length. A red shift of 623 pm was also observed from the start to the end of the writing process, itself related to an increase of the effective refractive index.

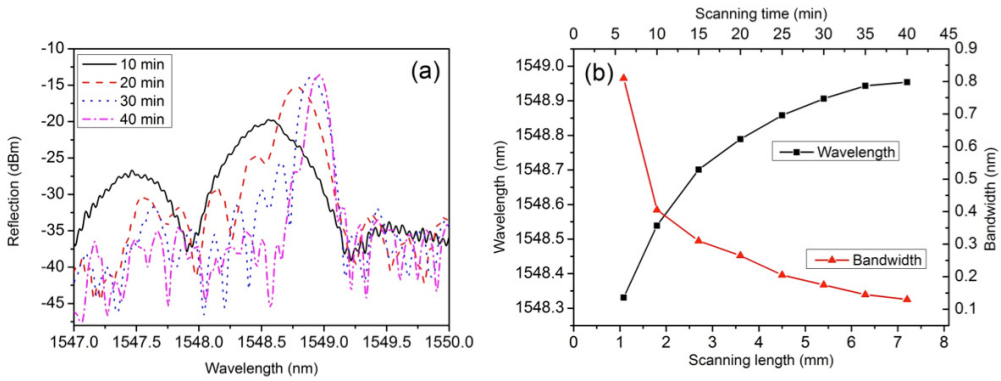

Fig. 4. Reflection band growth (a), wavelength and bandwidth (b) as a function of time during the writing process for a non-etched step-index 150 µm POF.

#210487 - $15.00 USD Received 21 Apr 2014; revised 9 Jul 2014; accepted 13 Jul 2014; published 25 Jul 2014

Figure 5 shows a comparison between the peak intensity evolutions for three POF diameter values, 150 µm (non-etched), 133 µm (5 minutes etched) and 108 µm (10 minutes etched), respectively. From this first experiment, we have empirically found that the highest peak intensity can be achieved in 133 µm diameter POF, with a ~6 dB enhancement compared to non-etched POFs. In terms of reflectivity, we get 97% for the 133 µm POF and only 25% for the 150 µm POF. These values were computed from the transmitted amplitude spectrum, after the photo-writing process. It is worth mentioning that these observations are only valid at the end of the writing process. For short gratings (1 mm), the reduced diameter could be the more efficient in terms of reflectivity. POFs with a smaller diameter are not stable during the writing process and the grating reflectivity does not grow continuously until saturation is reached. This is attributed to a too intense effective power in the fiber core, as the reduced PMMA thickness yields less attenuation. We believe that this limitation could be overcome by attenuating the laser output power. To decrease the fluence received by the fiber, we have tried inscriptions with faster scanning rates and have obtained the results depicted in Fig. 6.

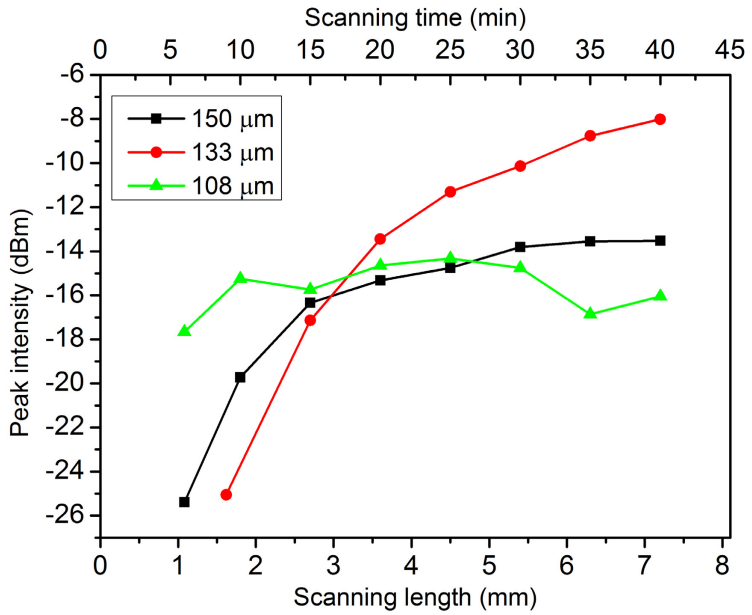

Fig. 5. Peak intensity evolution as a function of time during the writing process for three different POF diameters.

Figure 6 shows the reflective peak power of 6 mm long gratings (nearly 50 items) of different fiber diameters ranging between 107 and 156 µm right after the photo-inscription process with different laser scanning velocities (10 µm/s, 40 µm/s and 160µm/s). Taking into account the fiber diameter errors from fiber drawing and etching process, the diameter of each fiber section was measured precisely. Dispersion clearly appears on the raw data, resulting from uncontrolled coupling loss at the butt-connection between the POF section and the silica fiber pigtail. To evaluate this, we have tested different splices on a single FBG and have found that the different splicing conditions can affect the peak power by a maximum error of 0.6 dB. Nevertheless, general trends can be evaluated from this experiment, especially when making a linear fit of the raw data, as done in Fig. 6. Hence, it complements quite well the observations made in Fig. 5 in the sense that for the scanning speed at 10 µm/s, the gratings of maximum reflectivity were obtained for a cladding diameter close to 130 µm. And the grating reflectivity tends to decrease with the cladding diameter decreasing for a scan at 10 µm/s, again attributed to the too high fluence on the optical fiber. Increasing the scanning

#210487 - $15.00 USD Received 21 Apr 2014; revised 9 Jul 2014; accepted 13 Jul 2014; published 25 Jul 2014

speed can alleviate this effect. At 160 µm/s, the trend is opposite, with the grating reflectivity that tends to increase with a decrease of the fiber diameter. But in every case, the reflectivity remains smaller than for a slower scanning rate.

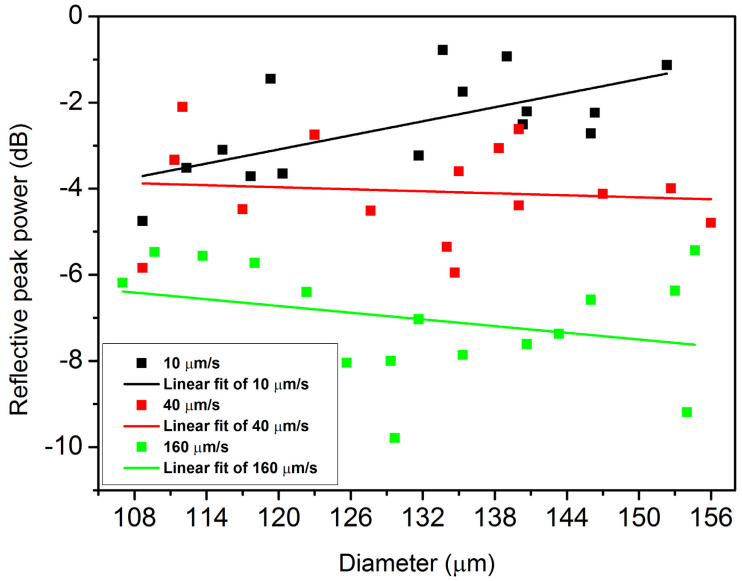

Fig. 6. Reflective peak power of 6 mm long gratings as a function of the fiber diameter for different scanning velocities (10 µm/s, 40 µm/s and 160µm/s).

Our observations clearly reveal that there is a trade-off between the fiber diameter and the scanning velocity (more generally related to the fluence) to produce highly reflective gratings. A deep investigation with some supporting theoretical analysis should be required to further support our experimental observations but it falls outside the scope of the present paper. Anyway, taking into account the huge number of photo-inscriptions reported in Fig. 5 and 6, we remain confident with respect to our claim that a cladding diameter decrease of ~12% remains the best to produce highly reflective gratings.

The three different diameter FBGs presented in Fig. 5 were then characterized in response to external stimuli to evaluate their differential sensitivities. The obtained results are reported and commented in the next sections.

3.2 Temperature sensing

Temperature characterization was conducted in an oven accurate to 0.1 °C inside a clean room of class 10,000 with the relative humidity controlled and kept constant to 30%. In order to preserve the POFs integrity, the maximum temperature investigated in this work was 47.3 °C. Temperature was adjusted by steps of ~4 °C. Figure 7 shows the evolution of the Bragg wavelength shift as a function of temperature for the three different FBG diameters mentioned above. Figure 7(a) shows nonlinear regressions (2nd order polynomial fit) on the raw data. Figure 7(b-d) show linear regressions on the same data, exhibiting more important standard deviations. The computed temperature sensitivities were equal to – 49.4 pm/°C ± 3.1 pm/°C, – 51.2 pm/°C ± 3.8 pm/°C and – 46.4 pm/°C ± 3.1 pm/°C for 150 µm, 133 µm and 108 µm FBGs, respectively. Hence, all three gratings behave similarly, taking into account the uncertainties on the temperature sensitivity computations.

#210487 - $15.00 USD Received 21 Apr 2014; revised 9 Jul 2014; accepted 13 Jul 2014; published 25 Jul 2014

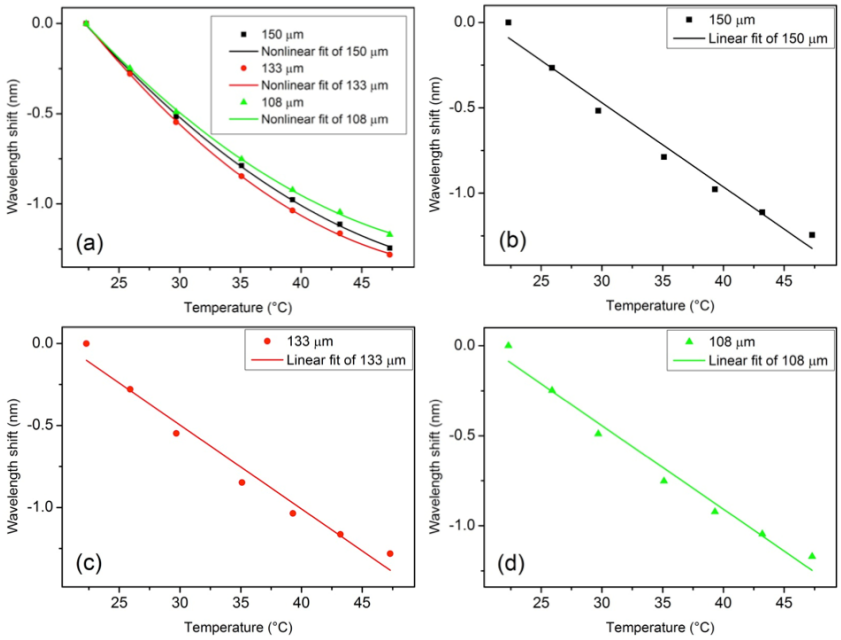

Fig. 7. Nonlinear fits of wavelength shifts with temperature for three different diameter FBGs (a); linear fits of wavelength shifts with temperature for diameter 150 μm (b), 133 μm (c) and 108 μm (d) POFs.

3.3 Axial tension sensing

Tension characterizations of FBGs were performed by hanging increasing weights at the end of the optical fibers. The computed tension sensitivities from a linear regression of the raw data were equal to 25.55 nm/N ± 0.12 nm/N, 29.89 nm/N ± 0.04 nm/N and 36.33 nm/N ± 0.13 nm/N for 150 μm, 133 μm and 108 μm FBGs, respectively, as depicted in Fig. 8. Hence, a cladding diameter reduction of ~12% (~30%) brings an enhanced axial tension sensitivity of 17% (42%), which can provide high resolution tension sensing. The maximum axial force that the 108 μm POF can sustain is ~0.15 N, very close to the one of the non-etched fiber.

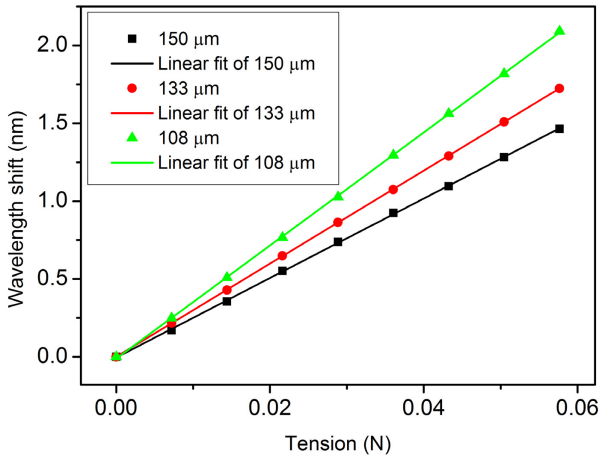

Fig. 8. Wavelength shift as a function of axial tension for three different diameters FBGs.

#210487 - $15.00 USD Received 21 Apr 2014; revised 9 Jul 2014; accepted 13 Jul 2014; published 25 Jul 2014

3.4 Refractive index sensing in saline solutions

Following the same procedure as the one described in [19], FBGs of different thicknesses were first inserted into a test tube of deionized water and in the meantime wavelength shifts were monitored. Within around four hours, FBGs were fully swelled by water and central wavelengths were stabilized after a red shift of ~5 nm. FBGs were then pulled out and inserted into another test tube of saline solution for one hour. Four samples of saline solution (1.3417, 1.3513, 1.3620 and 1.3716) were tested in the same conditions. Figure 9 shows the wavelength evolutions as a function of the refractive index of the saline solutions that were measured with an Abbe refractometer accurate to 10^{-4} RIU (refractive index unit). All three evolutions overlap and are nonlinear (2nd order polynomial fit), as already observed in [19]. To obtain a rough estimation of the sensitivity, a linear regression of the experimental data was made. It yields a sensitivity equal to – 44 nm/RIU ± 3 nm/RIU.

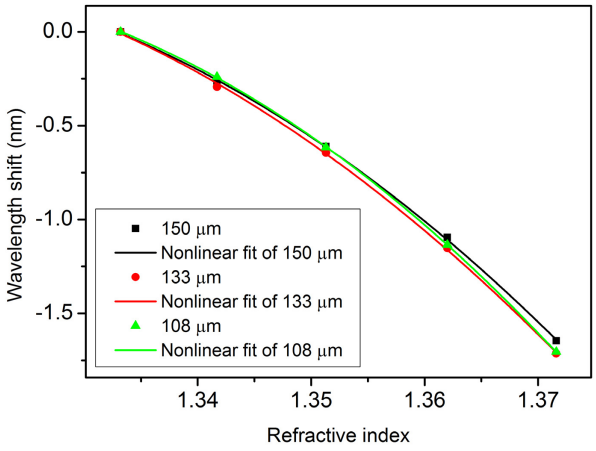

Fig. 9. Wavelength shift as a function of surrounding refractive index for three cladding diameters.

3.5 Estimation of photo-induced birefringence

The highest reflective FBGs obtained in 133 µm POFs were measured in transmission with polarized light. We have used an optical vector analyzer (OVA CTe from Luna Technologies) that was chosen for both its high wavelength resolution (1.25 pm) and its fast scanning rate (less than 1 s to analyze a range of a few tens of nm). Figure 10 depicts the insertion loss and polarization dependent loss (PDL) spectra measured by the OVA. As for uniform FBGs written in silica fiber [29], the PDL spectra exhibit two main peaks of nearly equal amplitude. They appear at wavelengths corresponding to the edges of the rejection band. Indeed, it has been shown that for FBGs, the PDL reduces to the ratio between the two orthogonal polarization modes (so-called x and y modes generated by birefringence effects) [30]. Hence, the PDL is minimum at the Bragg wavelength (where both x and y spectra are equal) and maximum at the edges (where the difference in amplitude between the x and y spectra is the maximum).

#210487 - $15.00 USD Received 21 Apr 2014; revised 9 Jul 2014; accepted 13 Jul 2014; published 25 Jul 2014

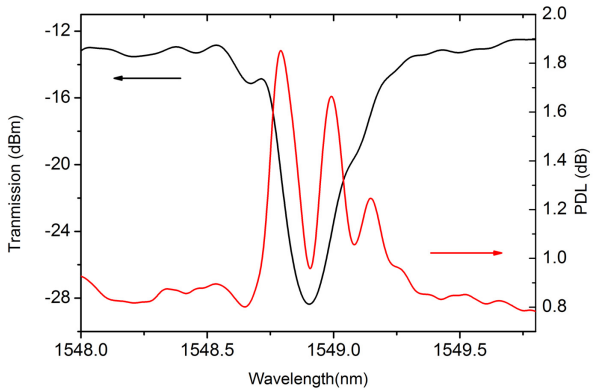

Fig. 10. Transmitted spectrum (black line) and polarization dependent loss (red line) for a 6 mm long FBG in 133 µm step-index POF.

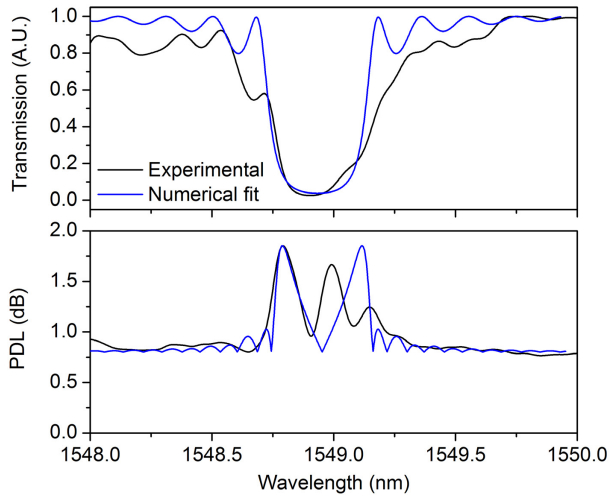

Fig. 11. Experimentally and numerically reconstructed transmitted amplitude and PDL curves for a 6 mm long FBG photo-inscribed in 133 µm step-index POF.

The photo-induced birefringence value has been estimated through a numerical fit of the experimental evolutions, using an inverse scattering program based on the Nelder-Mead simplex algorithm [27]. The transmitted amplitude spectrum was first adjusted to get the FBG physical parameters (length = 6 mm, refractive index modulation = 2.5×10^{-4} and grating period = 522 nm). With these parameters, the PDL curve was reconstructed and the birefringence value was optimized to minimize the difference between the experimental and simulated evolutions. Out of the rejection band, the PDL should lie around 0 dB, but here it is close to 0.8 dB, essentially due to the splices in addition to the intrinsic fiber birefringence. This value has been taken into account in the reconstruction process as an extra PDL value, which is not attributed to the photo-writing process. Figure 11 shows the experimental and numerically reconstructed evolutions and confirms the relatively good agreement between both evolutions. A discrepancy between experimental and simulated evolutions is noticed at the right-hand PDL peak, which is attributed to the spectral deformation of the rejection band on that side. In doing so, the photo-induced birefringence has been estimated to 7×10^{-6}. Thus, this measurement confirms that the side inscription process induces non-negligible photo-induced birefringence, as in the case of silica fibers [29,30]. This feature could be advantageously used for transverse force sensing.

#210487 - $15.00 USD Received 21 Apr 2014; revised 9 Jul 2014; accepted 13 Jul 2014; published 25 Jul 2014

4. Conclusion

In this work, we exploited Trans-4-stilbenemethanol-doped photosensitive step-index PMMA POFs. FBGs were inscribed at ~1550 nm by the scanning phase mask technique in POFs of different external diameters. We have demonstrated that a slight etching of step-index POFs (diameter decrease of ~12% of its initial value) makes possible the photo-inscription of highly reflective gratings (> 95%). Otherwise, the reflectivity is limited to 25% in pristine step-index POFs due to a strong absorption of the UV laser beam by PMMA. An enhancement of the axial tension was also reported for FBGs in reduced cladding POFs, while the temperature and surrounding refractive index sensitivities were kept constant compared comparing to non-etched POFs. Finally, through a measurement in transmission with polarized light, the photo-induced birefringence resulting from the lateral inscription process has been computed equal to 7×10^{-6}, which is comparable to the one generated in photosensitive silica fibers. This measurement paves the way to the further use of FBGs in POFs for transverse strain sensing.

Acknowledgment

This research has been conducted in the framework of the ERC (European Research Council) Starting Independent Researcher Grant PROSPER (grant agreement N° 280161 – http://www.umons.ac.be/erc-prosper) and the Actions de la Recherche Concertées research programme (PREDICTION project) supported by the Ministère de la Communauté française de Belgique—Direction générale de l'Enseignement non obligatoire et de la Recherche scientifique. C. Caucheteur is supported by the F.R.S.-FNRS.

#210487 - $15.00 USD Received 21 Apr 2014; revised 9 Jul 2014; accepted 13 Jul 2014; published 25 Jul 2014